15

Pulse Measurement Techniques Using an Acousto-Optic Programmable Dispersive Filter

Nicolas Forget and Thomas Oksenhendler
FASTLITE, Centre scientifique d'Orsay - Bât.503 - BP 45, 91401 Orsay
France

1. Introduction

Programmable spectral filters, such as acousto-optic programmable dispersive filters (AOPDF, Tournois (1997)) or spatial light modulators inserted in the Fourier plane of zero-dispersion lines (Froehly et al., 1983; Weiner, 2000), have opened up the field of ultrafast pulse shaping and given the ability to manipulate spectral amplitude and phase of broadband ultrashort pulses. These devices have found a great number of applications, among which are phase compensation in chirped-pulse amplification laser chains (Seres et al., 2003; Ohno et al., 2002; Verluise et al., 2000), coherent control experiments within atomic or molecular systems (Tkaczyk et al., 2008; Murphy et al., 2007; Veshapidze et al., 2007; Ogilvie et al., 2006; Yamada et al., 2005) and complex pulse shaping for photo-injectors (Garzella et al., 2006). Surprisingly, pulse shapers have mainly been used to control already well characterized ultrashort pulses but seldom to characterize these pulses themselves. And yet, pulse shapers provide a convenient way to perform quantitative, reliable and versatile pulse measurements.

A few pioneering works have already demonstrated that several of the existing pulse measurement techniques could be implemented with pulse shapers (Galler & Feurer, 2008; Sung et al., 2008; Forget et al., 2007; Oksenhendler et al., 2003; Monmayrant et al., 2003) and that new pulse characterization methods could even be invented (Forget et al., 2007; Grabielle et al., 2009; Lozovoy et al., 2004). The use of pulse shapers for ultrashort pulse metrology has already found practical applications, such as *in situ* pulse compression at the focus of high NA objectives in twophoton microscopy (von Vacano et al., 2006; 2007). Beyond specific applications, pulse shapers are expected to extend the robustness and dynamic range of the existing pulse characterization techniques. Indeed, all techniques suffer from specific weaknesses and cross-check can help to overcome the drawbacks, limitations or ambiguities related to a particular technique and to eliminate spurious results. Spectral phase interferometry for direct electric-field reconstruction (SPIDER) (Iaconis & Walmsley, 1998), for example, requires a precise calibration and determination of the relative delay between the two replicas. Such a requirement is much less stringent for the second-harmonic (SH) frequency resolved optical gating (FROG) technique. Conversely, SH-FROG suffers from time direction ambiguity and phase retrieval is not straightforward. Finally, these two methods are not equivalently robust with respect to complex pulse shapes. Cross-check between SH-FROG and SPIDER results is, however, often made difficult since it involves separate measurement devices, which multiplies the causes of

Source: Advances in Solid-State Lasers: Development and Applications, Book edited by: Mikhail Grishin,
ISBN 978-953-7619-80-0, pp. 630, February 2010, INTECH, Croatia, downloaded from SCIYO.COM

systematic experimental errors. As we shall demonstrate in this chapter, pulse shapers bring an elegant solution to this issue since both techniques can be implemented with the same device.

Despite the ever growing number of ultrafast pulse characterization techniques that have been proposed and demonstrated for four decades, it is possible to classify the various methods into a small number of categories (Wong & Walmsley, 1995). Since this classification is out of the scope of this paper, we will refer to a recent review paper by Walmsley and Dorrer (Walmsley & Dorrer, 2009). In brief, the characterization techniques relevant to the sub-picosecond pulse range fall within three general classes: spectrography, tomography and interferometry. Besides, all the techniques require at least one time-stationary filter and one time-nonstationary filter followed by an integrative detection. The most popular pulse characterization techniques dedicated to the shortest pulses use a nonlinear effect as a time-nonstationary filter. Most often, the chosen nonlinear effect is second harmonic generation (SHG), for practical reasons related to the efficiency of this process compared to other nonlinear effects. For the time-stationary filter, that is to say for the spectral filter, a set of conventional optics (beam-splitters, delay lines, dispersive materials) is used. Depending on the arrangement and nature of these optics, the pulse retrieval algorithm will differ, giving rise to different pulse characterization techniques. It is of the greatest interest to note that, following the formalism developed by Walmsley and Dorrer, any pulse characterization technique could be implemented with a minimal setup, including no more than a couple of spectral filters and nonlinear stages.

In this chapter we review, both theoretically and experimentally, the practical adaptation of pulse measurement techniques to a setup including one *single* phase and amplitude pulse shaper and one *single* nonlinear stage. Special attention will be drawn on their implementation with AOPDFs, a class of bulk and compact pulse shapers particularly well adapted to this quantitative use. We will focus on pulse durations ranging from a few tens to a few hundreds of fs (20fs-1ps) over the entire visible to near-infrared spectral range (550-1600nm). Section 2 presents the key features of pulse-shaper-based techniques whereas sections 3 to 5 are dedicated to FROG-inspired and SPIDER-inspired techniques. Section 6 will deal with the extension of these techniques to near UV (266-400nm).

2. Formalism and experimental setup

2.1 Representation of pulses fields

Assuming the light field is linearly polarized, the electric field $\varepsilon(t)$ may be described as the real part of an analytic signal $E(t)$:

$$\varepsilon(t) = \mathrm{Re}\{E(t)\} \tag{1}$$

$E(t)$ is a complex function of time with a compact support within some time interval [-T,+T] and can be expressed in terms of carrier and envelope as follows:

$$E(t) = A(t)e^{-i\omega_0 t} \tag{2}$$

where ω_0 is the carrier angular frequency and $A(t)$ is the complex time amplitude. The Fourier transform of $A(t)$, noted $A(\omega)$, is referred to as the complex spectral amplitude of the pulse. Both $A(t)$ and $A(\omega)$ can be described in terms of modulus and phase. The square of the

complex time amplitude, $I(t) = |A(t)|^2$, is the time-dependent instantaneous power. $I(\omega) = |A(\omega)|^2$ is referred to as the spectral intensity.

2.2 Spectral filters

All the optically *linear*[1] and *time-stationary*[2] operations on a pulse can be described by a complex spectral filter or, equivalently, by an impulse time response, these two functions being conjugated by Fourier transform. If $A_{in}(\omega)$ is the input spectral amplitude of an optical pulse, then the spectral amplitude at the output of an optical element characterized by the spectral filter $H(\omega)$ is equal to the *product* of $A_{in}(\omega)$ and $H(\omega)$:

$$A_{out}(\omega) = H(\omega)A_{in}(\omega) \tag{3}$$

Conversely, if $A_{in}(t)$ is the time complex amplitude of the input pulse and $H(t)$ is the time impulse response of the optical element, then the complex time amplitude of the output pulse is given by the convolution of $A_{in}(t)$ and $H(t)$:

$$A_{out}(t) = H(t) \otimes A_{in}(t) \tag{4}$$

The spectral filters of some of the most useful operations in optics are given in Table 1.

Description	Time-domain definition	Spectral filter
Attenuation	$A_{out}(t) = kA_{in}(t)$	k
Phase offset	$A_{out}(t) = e^{i\theta}A_{in}(t)$	$e^{i\theta}$
Optical delay	$A_{out}(t) = A_{in}(t-\tau)$	$e^{-i(\omega-\omega_0)\tau}$
Chirp	-	$e^{i\phi_2(\omega-\omega_0)^2}$

Table 1. Spectral filters associated with some common optical operations.

Any combination of linear operations can be described by a single spectral filter. For example, the operation "create two pulse replicas with an optical interpulse delay τ and a relative phase offset of $\pi/4$" is described by the spectral filter:

$$H(\omega) = 1 + e^{i\frac{\pi}{4}}e^{-i(\omega-\omega_0)\tau} \tag{5}$$

or equivalently by the time response function:

$$H(t) = \delta(t) + e^{i\frac{\pi}{4}}e^{i\omega_0\tau}\delta(t-\tau) \tag{6}$$

where $\delta(t)$ stands for the Dirac function.

[1] Linear is to be understood in the mathematical sense. An application f is linear if and only if for any values (a, b) of a given vectorial space and for any values of $k \in \mathbb{C}$, $f(a+k.b) = f(a) + k.f(b)$ and $f(0) = 0$.

[2] An operation which effects do not vary with the choice of the origin of time (an operation invariant by translation in time). For example, the operation "delay" is stationary but the operation "multiplication by a sinus" is not stationary.

It must be noted that the *optical delay* used in the former paragraph corresponds mathematically to a pure translation of the electric field $\varepsilon(t)$ along the time dimension. But this is not the case for the time-dependent amplitude (envelope function) $A(t)$ of the pulse. Indeed, the spectral filter associated with a pure translation in time of the amplitude - which we will call a *pure delay* - writes $H(\omega) = e^{-i\omega\tau}$, which is different from the optical delay $H(\omega) = e^{-i(\omega-\omega_0)\tau}$. Physically, an *optical delay* corresponds to a *pure delay* plus a phase shift of the carrier-envelope (Albrecht et al., 1999).

As it has been mentioned already in this chapter, pulse shaper devices offer the possibility to mimic almost any set of conventional optics. However, this statement must be mitigated, since pulse shaping devices require both input and output to be single beam (one beam in - one beam out) and linearly polarized. The equivalent optical setups are thus limited to the ones preserving the space profile and the polarization state. These constraints limit, in turn, the number of pulse measurement techniques that are transposable to pulse shapers, since many techniques require either two shaped beams or, which is almost equivalent, two shaped polarization states. We will hereafter distinguish the measurement techniques requiring a *single* spectral filter from the techniques requiring *two* spectral filters.

To extend the number of adaptable characterization techniques, it is convenient to use in combination with a pulse shaper a polarization multiplexer to enable not only the control of the spectral phase and amplitude but also of the output polarization state as a function of frequency. An example of such a polarization multiplexer is given in subsection 2.4.

2.3 Pulse shaping device

As mentioned before, pulse shaping devices such as the AODPF can be viewed as generic programmable spectral filters since their spectral phase and amplitude can be almost arbitrarily defined. These devices are nevertheless characterized by a finite *bandwidth* and a finite spectral *resolution*. The bandwidth refers to the maximal spectral range over which the device can operate, which might be limited by the absorption edges of the constitutive material, optical coatings or by any other physical mechanism leading to a drop of throughput. Typical bandwidth values for the AOPDF cover about one octave from the visible (>530nm) to the near infrared (<3μm), for example, 550nm-1100nm. As far as pulse measurement is involved, this limits the minimal duration of the measurable ultrashort pulses to a few optical cycles.

The spectral resolution of a pulse shaper refers to the minimal spectral feature, in both amplitude or phase, that can be controlled. Although spectral resolution can be expressed in terms of full width at half maximum (FWHM), it is much more convenient to express the spectral resolution in the conjugate space, that is in the time domain. As a matter of fact, all pulse shaping devices have a finite impulse time response which vanishes outside of a given time window $[0,T_{\max}]$. This window will be referred to as the *pulse shaping window*. In application of the sampling theorem, the spectral resolution of a pulse shaper is proportional to the inverse of the pulse shaping window width. It is clear that a finite spectral resolution implies, in the context of pulse characterization, that the largest measurable pulse durations will be limited to a fraction of the pulse shaping window. For an AOPDF, the pulse shaping window depends on the thickness of the acousto-optic crystal and ranges usually from 3ps to 15ps. The experimental data showed in the following sections were recorded by using a ~7ps pulse shaping window, which corresponds to a FWHM spectral resolution of better than 150GHz (about 0.3nm at 800nm).

Other features, however less stringent, distinguish pulse-shaper-generated spectral filters from their conventional counterparts. For example, the spectral filter is not static on long time scales (tens of μs to tens of ms) and the pulse shaping device must be triggered.

2.4 Experimental setup

2.4.1 Optical layout

All the experiments reported in section 3 and section 4 were performed with the same optical layout: an AOPDF, an optional 6mm Calcite retardation plate for polarization multiplexing, a focusing lens, a second harmonic generation stage (thin BBO crystal) and a miniature spectrometer.

The heart of the system is an acousto-optic birefringent crystal of Paratellurite (TeO_2). The action of the AOPDF is based on a quasi-collinear interaction between an optical beam and an acoustic beam (Tournois, 1997). Through the process of acousto-optic diffraction, this interaction gives rise to a diffracted beam when suitable phase matching conditions are met. In the time domain and for low values of acoustic power density, this crystal performs a convolution between the complex amplitude of the input optical pulse and that of the acoustic pulse. In the spectral domain, this device acts as a programmable spectral filter. Without Calcite plate and assuming a perfectly phase-matched SHG, the signal collected by the spectrometer is given by:

$$I(\omega) \propto \left| \int \left[H(t) \otimes A(t) \right]^2 e^{2i\omega_0 t} e^{-i\omega t} dt \right|^2 \tag{7}$$

where $H(t)$ is the time impulse response of the considered spectral filter.

2.4.2 Polarization multiplexing

When polarization control of the output pulses is required (two-filter techniques), a 6mm thick retardation plate made of Calcite is inserted between the AOPDF and the SH crystal. This birefringent plate is cut such that its optical axis is perpendicular to the direction of incidence and orientated at 45 degrees to the polarization plane of the diffracted beam. With this setup, the fraction of the shaped pulse which is extraordinary polarized with respect to the Calcite crystal, is delayed with respect to the ordinary polarized part. This differential delay, noted τ_c, is proportional to the birefringence of the Calcite crystal and to the thickness of the plate. As depicted in Figure 1, if the AOPDF is set to produce two consecutive pulses of adjacent but non-overlapping time supports $A_1(t)$ and $A_2(t)$ and if the birefringent group delay is chosen to match that of the time delay between $A_1(t)$ and $A_2(t)$, then, after propagation through the Calcite plate, four pulses will emerge: two ordinary polarized pulses and two extraordinary pulses. Among them, the only overlapping pulses are the ordinary projection of $A_2(t)$ and the extraordinary projection of $A_1(t)$. If the principal polarization planes of the type II SHG crystal are orientated parallel to those of the Calcite plate, the type II SHG signal will be proportional to the product of these two projections. Mathematically, the spectral filter required to produce the pulse replicas is:

$$H(\omega) = H_1(\omega) + H_2(\omega) e^{-i\omega\tau_c} \tag{8}$$

Assuming a perfect phase matching in a type II second harmonic generation stage, the SH signal collected by the spectrometer will then be equal to:

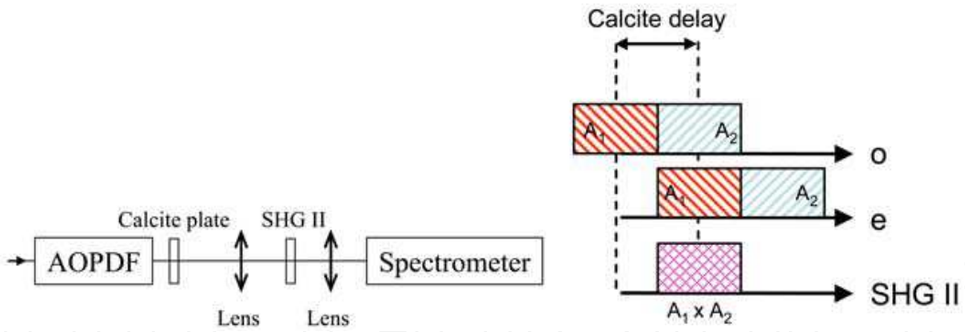

Fig. 1. a) Optical setup. b) Principle of polarization multiplexing.

$$I(\omega) \propto \left| \int \left[H_1(t) \otimes A(t) \right] \left[H_2(t) \otimes A(t) \right] e^{2i\omega_0 t} e^{-i\omega t} dt \right|^2 \tag{9}$$

where $H_1(t)$ and $H_2(t)$ are the time impulse responses of the spectral filters $H_1(\omega)$ and $H_2(\omega)$. The use of this polarization multiplexing technique comes at some cost however: the principal polarization planes in the SHG and Calcite crystals must be aligned with high precision, the effective pulse-shaping window is reduced by a half, and a half of the energy of the shaped pulses does not contribute to the SH generation.

2.4.3 Dispersion precompensation

It is well-known that propagation through thick dispersive media drastically modifies the spectral phase of broadband pulses. Therefore, in order to characterize the input pulses, it is required to compensate for both the dispersion of the AOPDF crystal and focusing lens. When the Calcite plate is used, it is also necessary to compensate for the mean and differential dispersions. As a result, for all measurements, the spectral filter will be defined as the product of the "measurement" filter $H(\omega)$ and a precompensation filter $\Pi(\omega)$. $\Pi(\omega)$ is defined as follows: $|\Pi(\omega)|$ is a supergaussian function of order 6, defining the bandwidth of the measurement, and $\arg(\Pi(\omega))$ is equal to the opposite of the total dispersion of all the optical elements of the device. It must be noted that $\Pi(\omega)$ uses part of the pulse shaping capability. It also limits the minimal measurable pulse duration (~10fs for a gaussian spectrum), since the AOPDF cannot compensate itself over a bandwidth larger than ~300nm. In the following section, $\Pi(\omega)$ will be dropped out for the sake of clarity.

3. Two-filter measurements

A first class of pulse measurement methods relies on a *spectrographic* measurement, that is on the analysis of the spectral content of a time-slice of the pulse to be characterized. The most popular techniques belonging to this class are the multiple flavors of Frequency-Resolved Optical Gating (FROG) (Trebino et al., 1997). In FROG-related techniques, the measured quantity is the spectrally-resolved autocorrelation or cross-correlation function of the pulse. From this bi-dimensional data (spectrum as a function of time delay between pulse replicas), the spectral phase and amplitude can be retrieved by an iterative algorithm. In practice, a SH-FROG setup consists of an interferometer producing two pulse replicas of the pulse to be characterized, a second harmonic crystal and a spectrometer. Since FROG open-space setups use two non collinear beams or two collinear but perpendicularly

polarized beams (Fittinghoff et al., 1998; Gallmann et al., 2000), it is clear that FROG is a two-filter measurement method. It is worth noting that FROG does not exhaust the class of spectrographic techniques. The STRUT technique for example, also belongs to this class and has been implemented with a pulse shaping device (Galler & Feurer, 2008).
A second class of measurement techniques relies on an *interferometric* measurement. In this case, the experimental data is unidimensional and the spectral phase is encoded as a spectral or temporal beating signal. The most popular member in this class is SPIDER. As FROG, usual practical implementations of SPIDER make use of two beams.
In this section, we will focus on the implementation of FROG and SPIDER, as two-filter methods, in pulse-shaper-based measurement devices. All the reported data were acquired with the polarization multiplexing setup.

3.1 SH-FROG

For intensimetric FROG, the signal collected by the spectrometer is equal to:

$$I_{\mathrm{FROG}}(\tau,\omega) \propto \left| \int A(t)A(t-\tau)e^{2i\omega_0 t}e^{-i\omega t}dt \right|^2, \tag{10}$$

The corresponding spectral filter is therefore:

$$H_{\mathrm{FROG}} = (\tau,\omega) = 1 + e^{-i\omega(\tau+\tau_c)} \tag{11}$$

where τ_c stands for the differential group delay of the Calcite plate. This function being a two-dimensional function, the measurement cannot be made single-shot with the studied setup. However, by using a discrete number of time delays τ, the FROG trace can sampled in the time direction and used to retrieve the spectral phase and amplitude of the complex envelope $A(t)$.

3.1.1 Trace features

A FROG trace can be divided into three areas: small, large and intermediate delays. In the small delay area, that is to say close to zero delay, the signal is maximal and corresponds to the SHG signal of the pulse:

$$I_{\mathrm{FROG}}(\tau = 0,\omega) \propto I_{\mathrm{SH}}(\omega) \tag{12}$$

At sufficiently large delays, the pulse replicas do not overlap anymore in time and the FROG signal vanishes:

$$I_{\mathrm{FROG}}(\tau \to \infty,\omega) = 0 \tag{13}$$

In the intermediate range, the FROG trace cannot be expressed simply but must remain symmetric with respect to the origin of time. Indeed, changing τ into $-\tau$ in Equation 10 doesn't change the value of the integral:

$$I_{\mathrm{FROG}}(-\tau,\omega) = I_{\mathrm{FROG}}(\tau,\omega) \tag{14}$$

This particular feature implies that FROG method is inherently insensitive to the direction of time, which is known as the "time ambiguity" of FROG traces and retrieved pulse temporal profiles.

3.1.2 Retrieval algorithm

FROG traces cannot be analytically inverted to retrieve the spectral phase (and amplitude) of the corresponding pulse. However, some efficient iterative pulse retrieval algorithms exist, and the Principal Component Generalized Projects algorithm (PCGPA, DeLong et al. (1994); Kane et al. (1999); Reid (1999)) is one of the most powerful among all published algorithms.

Most often the raw experimental data have to be processed and formatted prior to the application of the PCGPA algorithm. In particular, the background signal must be removed with care. Indeed, as the FROG algorithm is based on a time-frequency description, a constant background would be interpreted as continuous (single-frequency) contribution to the signal. Once the background is removed, it is mandatory to re-sample and/or extrapolate the spectra in order to satisfy the Nyquist-Shannon sampling theorem.

When a pulse shaper is used to generate the time delay between the two pulse replicas, the delay step and the number of points along the time direction can be arbitrarily defined. It must be noticed, that the spectral grid on which the spectra must be sampled is only set by the delay span of the measurement. Let the sampled delays be:

$$\tau_k = \tau_{\max} \frac{(k-N)}{N} \text{with } k = 1..(2N-1) \tag{15}$$

The SHG spectra will then have to be re-sampled on the frequency grid:

$$\nu_k = 2\nu_0 + \Delta\nu \frac{(k-N)}{N} \text{with } k = 1..(2N-1) \tag{16}$$

where $\Delta\nu$ is the Nyquist frequency of the delay sampling:

$$\Delta\nu = \frac{2}{\tau_{\max}} \tag{17}$$

and ν^0 is the central frequency of the fundamental pulse (i.e. its carrier frequency). From Equation 17 it follows that the *spectral resolution* of a FROG measurement is inversely proportional to the maximum explored time delay. Since both the delay excursion and the delay step size can be arbitrarily chosen within the pulse shaping window of the AOPDF, the spectral resolution of the measurement can be adapted to the pulse to be measured. Besides, with an AOPDF, the precision on the interpulse delays is estimated to be better than ~100as (10^{-16}s), which is about one magnitude lower than the optical cycle period in the visible and IR spectral ranges.

3.1.3 Experimental example

We used as test pulses a leakage (1μJ) from a kHz amplified system delivering pulses of ~100fs at 800nm. The leakage beam was sent into a 25mm AOPDF and the diffracted beam was focused by a plano-convex lense (f=75mm) in a 100μm-thick BBO crystal cut for a type II SHG at 800nm. The generated SHG beam was refocused at the input of a miniature spectrometer (Avantes, 3648 pixels, 700-900nm). 65 equidistant time delays covering the [-1000fs, 1000fs] interval were used for this measurement. Figure 2 shows the experimental FROG trace, the reconstructed FROG trace, the retrieved spectral phase and amplitude and the retrieved time intensity.

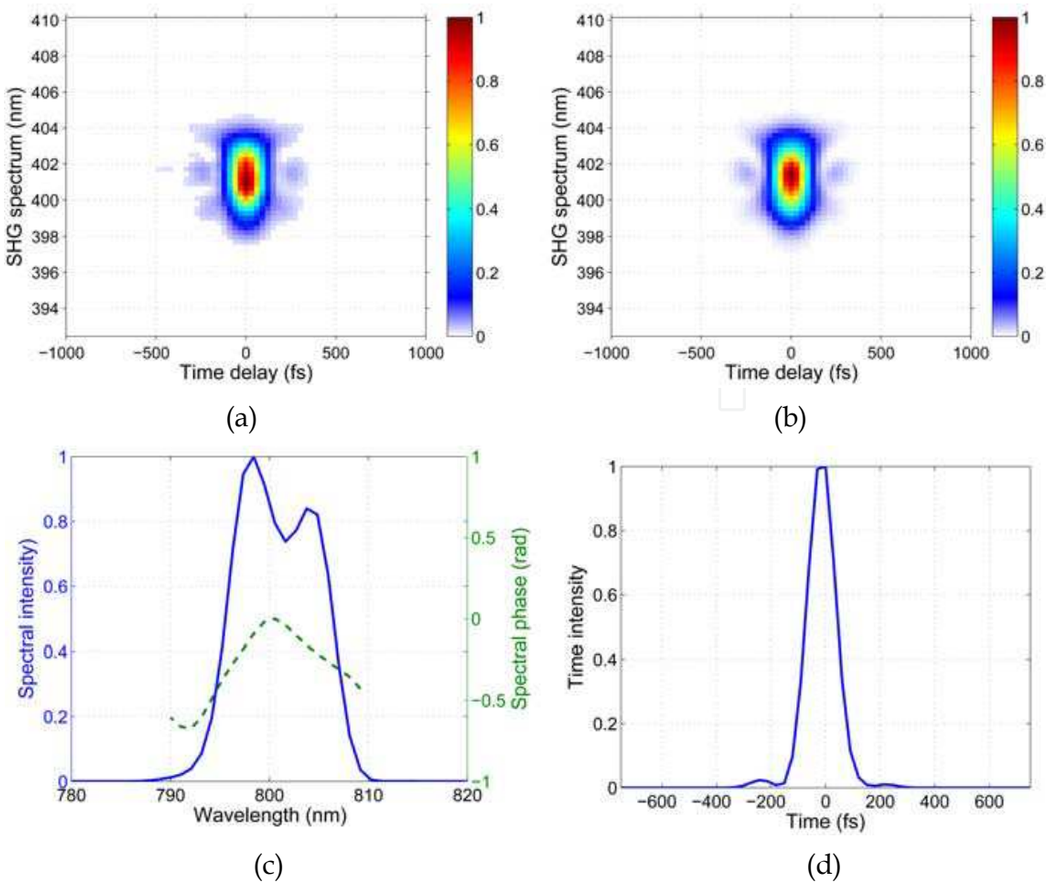

Fig. 2. a) Experimental FROG trace. b) Reconstructed FROG trace. c) Retrieved spectrum and spectral phase. d) Retrieved time intensity (123fs FWHM).

3.2 SPIDER

Contrary to the FROG technique, SPIDER doesn't allow the reconstruction of the spectral intensity (i.e. the spectrum must be measured independently). However, it provides an analytic and unambiguous determination of the spectral phase. SPIDER is based on shearing interferometry in the optical frequency domain, which means, on the interference pattern created by two frequency-shifted replicas of the pulse. Let $A(\omega) = \sqrt{I(\omega)}\exp(i\varphi(\omega))$ be the spectral complex amplitude of a broadband optical pulse, and let $A(\omega + \delta\omega)$ be the spectrally shifted replica of $A(\omega)$. The interference pattern between $A(\omega)$ and $A(\omega + \delta\omega)$, as recorded by a square-law detector, is:

$$S(\omega) = I(\omega) + I(\omega + \delta\omega) + 2\sqrt{I(\omega)}\sqrt{I(\omega + \delta\omega)}\cos\left[\varphi(\omega) - \varphi(\omega + \delta\omega)\right] \tag{18}$$

The phase difference can be easily and algebraically extracted from the interference pattern using standard Fourier processing techniques. The spectral phase of the field, $\varphi(\omega)$, can then be reconstructed by concatenation or integration.

In a conventional SPIDER setup, two replicas of the pulse separated by a delay τ are mixed in a nonlinear crystal with a chirped pulse having a large second-order dispersion. Because

of the linear relation between time and instantaneous frequency in the chirped pulse, the instantaneous frequencies are constant during the interaction with each of the short replicas but differ by the spectral shear. The nonlinear interaction shifts the complex amplitudes of the replicas of the initial pulse by two different frequencies separated by a frequency shift $\delta\omega$. Measurement of the phase difference between the two sheared replicas by use of Fourier transform spectral interferometry (FTSI) gives access to the quantity:

$$\phi_{\text{SPIDER}}(\omega) = \omega\tau + \varphi(\omega + \omega_0) - \varphi(\omega + \omega_0 + \delta\omega) \tag{19}$$

The phase of the initial pulse is then obtained in three steps: substraction of the linear term $\omega\tau$, global shift by ω_0 along the frequency axis, and concatenation/integration of the phase by steps of $\delta\omega$. This inversion algorithm is thus totally algebraic and does not rely on iterative procedures.

Despite its numerous advantages (single-shot, analytic, unambiguous...), the SPIDER technique usually requires several precise calibrations. Indeed, the values of the interpulse delay τ, the global shift ω_0 and the spectral shear $\delta\omega$ are key parameters. Although these parameters can be measured by several means, using a bulk pulse shaper such as the AOPDF to produce the pulse replicas and the chirped pulse brings an elegant solution to the calibration issue:

- the interpulse delay is known, without any need for external calibration,
- the global shift is known with high accuracy,
- all the parameters (interpulse delay and spectral shear) can be changed at will.

This measurement is the exact equivalent of the classical SPIDER optical setup: the AOPDF generates two identical pulse replicas of the input pulse and one highly chirped narrowband pulse which is obtained by frequency filtering. The Calcite plate is used to rotate the polarization of the chirped pulse so that the pulse replicas and the chirped pulse can experience a background-free sum-frequency generation in a type II BBO crystal.

The experimental measurements displayed in this section were performed at ~800nm, at the output of an amplified kHz Ti:Sapphire laser system. About 10μJ of energy was sampled from the main beam and used for the pulse measurement. The AOPDF was a 25mm TeO_2 crystal and the SHG crystal was a 20μm-thick BBO crystal cut for a type II phase matching. The interpulse delay was set to 500fs and the spectral shear to 1.2nm at 800nm. Figure 3 shows the raw SPIDER spectrum together with the retrieved spectral phase and time intensity.

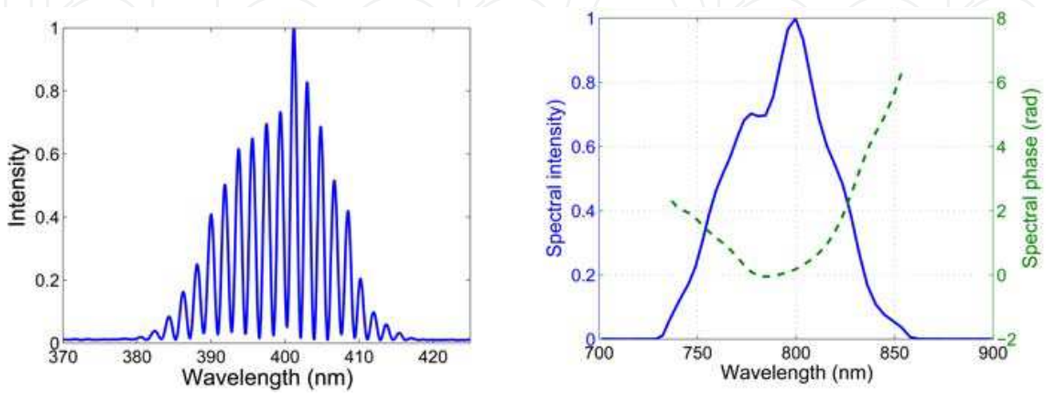

Fig. 3. a) Experimental single-shot SPIDER spectrum. b) Extracted spectral amplitude and phase. Retrieved pulse duration was 28fs FWHM.

4. Single filter measurements

As it was pointed out in section 3, SH-FROG and SPIDER are intrinsically two-filter pulse measurement techniques. Some workarounds, such as polarization multiplexing, can be found to implement these techniques with a single pulse shaper. However, it is much more convenient to use single-filter variants of these techniques: type I phase matching can be used instead of type II and no additional birefringent crystal is required, which removes the drawbacks expressed in 2.4.2. In this section we introduce, for the first time, single-filter variants of SHFROG and SPIDER.

4.1 Interferometric FROG

Interferometric FROG (iFROG) is the most simple variant of the FROG technique to be implemented with a pulse shaping device. The optical setup of iFROG is a Michelson interferometer, followed by a second harmonic generation stage and a spectrometer (Amat-Roldan et al., 2004; 2005). The signal collected by the spectrometer is then equal to:

$$I_{\mathrm{iFROG}}(\tau,\omega) \propto \left| \int \left(A(t) + A(t-\tau) e^{i\omega_0 \tau} \right)^2 e^{2i\omega_0 t} e^{-i\omega t} dt \right|^2 \tag{20}$$

where ω_0 is a the optical carrier frequency. Comparing formula 20 and 7, leads to the following spectral filter:

$$H_{\mathrm{iFROG}}(\omega) = 1 + \exp -i\left[(\omega - \omega_0)\tau \right] \tag{21}$$

Given the order of magnitude of ω_0 (several $10^{15} Hz$), the oscillation period is of the order of a few fs. As a result, it is not always possible to sample both correctly the autocorrelation signal over large delay ranges and keep a small number of sampling points. A Gaussian pulse of 200fs FWHM at 800nm, for example, requires a scanning range of ±600fs, which corresponds to a minimal number of sampling points of ~900. By using a pseudo-carrier of angular frequency Ω, this number can be reduced greatly without any loss of information. Such a substitution is impossible when using a mirror-based Michelson interferometer. However, with a pulse shaper, this is possible and for the sake of generality, we will consider the following class of filters:

$$H_{\Omega}(\omega,\tau) = 1 + \exp -i\left[(\omega - \Omega)\tau \right] \tag{22}$$

Compared to FROG traces, iFROG traces exhibit oscillations with respect to delay, with a period equal to the period of the pseudo-carrier (Galler & Feurer, 2008). This feature is equivalent to that of conventional interferometric autocorrelators, for which $\Omega = \omega_0$. As a FROG trace, a iFROG trace can be divided into three areas: small, large and intermediate delays. In the small delay area, that is to say close to delay zero, the signal is maximum and corresponds to the SHG signal of the pulse.

$$I_{\mathrm{iFROG}}(\tau = 0, \omega) \propto 16 I_{\mathrm{SH}}(\omega) \tag{23}$$

At sufficiently large delays, the pulse replica do not overlap any more in time and the iFROG signal is equal to the interference pattern of the time-shifted SHG pulses:

$$I_{\mathrm{iFROG}}(\tau \to \infty, \omega) \propto 4 I_{\mathrm{SH}}(\omega) \cos^2\left(\delta\omega\tau / 2 - \Omega\tau \right) \tag{24}$$

where $\delta\omega = \omega - 2\omega_0 + \Omega$ is the frequency offset from the frequency carrier of the SHG signal. As a matter of fact, the iFROG signal does not vanish for large delays as for the FROG signal.
For intermediate delays, the iFROG signal is more complex. It can be expressed as a function of the centered FROG signal:

$$E^c_{\mathrm{FROG}}(\tau,\omega) = \int A(t-\tau/2)A(t+\tau/2)e^{i(2\omega_0-\omega)t}dt \tag{25}$$

The iFROG signal is then equal to:

$$I_{\mathrm{iFROG}}(\tau,\omega) \propto I_{\mathrm{SH}}(\omega)\cos^2\left(\frac{\delta\omega\tau}{2}-\Omega\tau\right) + 4I^c_{\mathrm{FROG}}(\tau,\omega)$$

$$+8\cos\left(\frac{\delta\omega\tau}{2}-\Omega\tau\right)\mathrm{Re}\left[E^{\star}_{\mathrm{SH}}(\omega)E^c_{\mathrm{FROG}}(\tau,\omega)\right] \tag{26}$$

This expansion shows that the iFROG signal is the sum of three terms: a SH component, a FROG component and a cross-term. iFROG traces must be, - as all FROG type traces -, symmetric with respect to delay zero. Besides, the autocorrelation trace (i.e. the iFROG trace integrated along the spectral coordinate) exhibits the following features: the signal is positive, reaches a maximum at zero delay and becomes constant at large delays. Besides, the ratio between the signals at zero delay and large delays is equal to 8.
As for FROG, the delay range must be much greater than the pulse duration. More precisely, the maximum delay must be chosen so that the electric field at such delays is truly zero. For example, for a 30fs gaussian pulse, the maximum delay must be set to at least 120-150fs. A rule of the thumb is to choose a value which is equal to 4-5 times the expected pulse duration. The minimum number of points to acquire is a function of the pulse complexity. A good estimation of the pulse complexity is given by the time-bandwidth product of the pulse. Arule of the thumb to choose the right number of points is to multiply the expected time-bandwidth product by 128.

4.1.1 Phase retrieval algorithm

Several phase retrieval algorithms for iFROG have been published already. Most of them, however, were developed for the iFROG with $\Omega = \omega_0$ and did not consider the new degree of freedom given by the ability to choose $\Omega \neq \omega_0$. Mainly, there are two different approaches. From Equation 26 it is clear that if the product $\Omega \times \Delta\tau$, where $\Delta\tau$ is the time support of the measured pulse, is greater than a few units, then the three components of the iFROG signal (SHG, FROG term and cross-term) can be isolated by Fourier filtering. A first method consists in extracting the FROG term (i.e. the low frequency term) and then retrieving the spectral phase and amplitude by using the PCGPA algorithm (Stibenz et al., 2006; Stibenz & Steinmeyer, 2005). A second method consists in using the cross-term (i.e. the term oscillating at $\pm\Omega$), from which the spectral phase can be analytically extracted (MEFISTO technique, Amat-Roldan et al. (2004; 2005)).

4.1.2 Experimental demonstration

The experimental demonstration of iFROG was carried at the SHG output (~600nm) of a collinear optical parametric amplifier (OPA) pumped by a Ti:Sapphire amplified system.

About 1μJ of energy was sampled from the main beam and used for the pulse measurement. The AOPDF was a 25mm TeO_2 crystal and the SHG crystal was a 20μm-thick BBO crystal cut for a type I phase matching. The focusing lens was achromatic with a focal length of 50mm and the spectrometer had a 0.05nm resolution (AvaSpec-2048 from Avantes). Figure 4 displays the raw experimental iFROG trace and iFROG autocorrelation together with the filtered FROG trace and the corresponding reconstructed FROG trace.

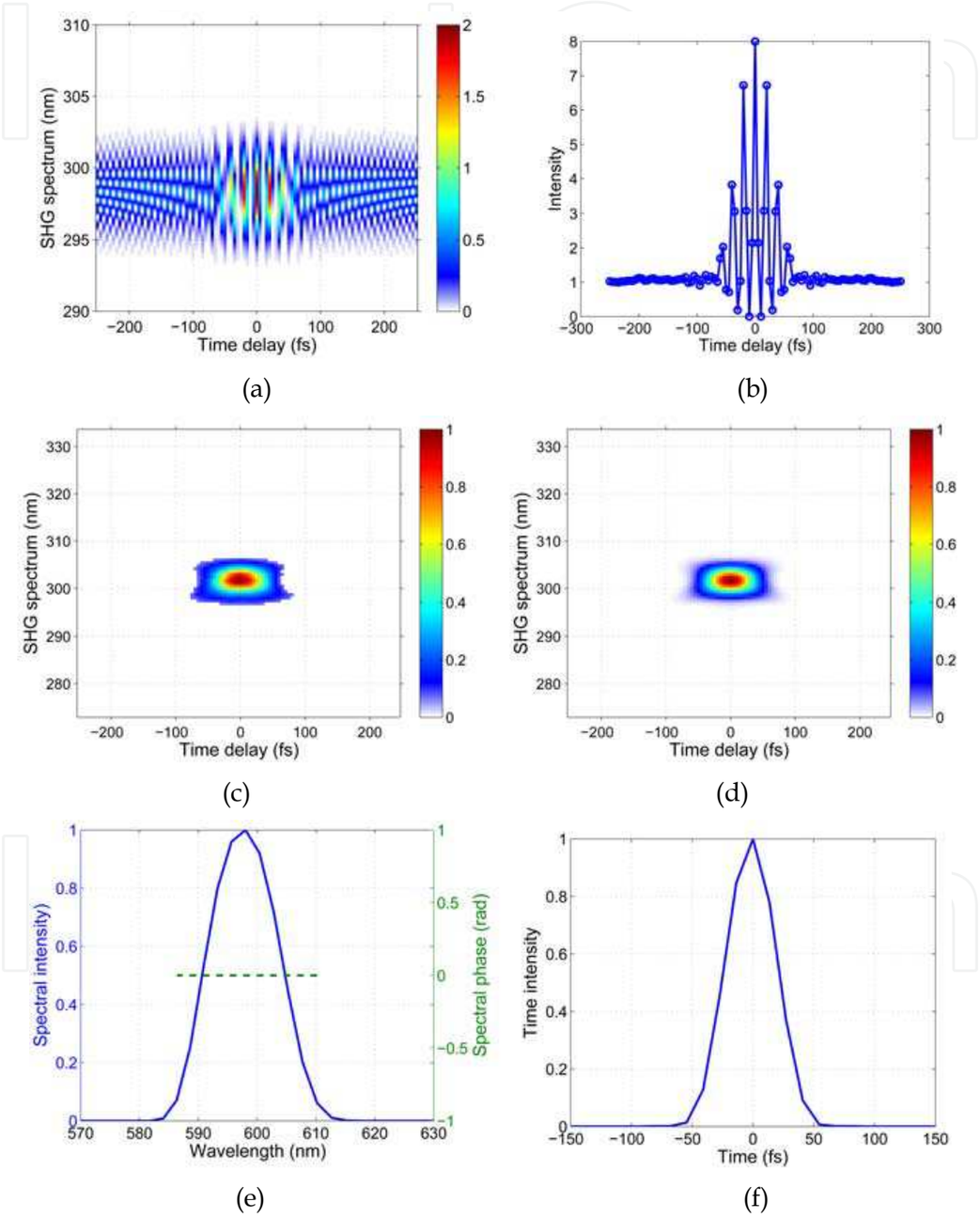

Fig. 4. a) Experimental iFROG trace. b) Experimental iFROG autocorrelation. c) Filtered FROG trace. d) Retrieved FROG trace. e) Retrieved spectral phase and intensity. f) Retrieved time intensity.

4.2 Baseband interferometric FROG

In the limit Ω→0, the phase retrieval algorithm detailed in the previous section doesn't work anymore and another algorithm is required. Far from being pathologic, this variant of iFROG is highly interesting from a practical point of view. Indeed, at Ω = 0, the iFROG trace is free from fast oscillations and therefore requires a minimal number of sampling points in the time direction. Given these properties we call this technique *baseband interferometric FROG* or bFROG. What is more, the obtained traces are very close to that of intensimetric SHG-FROG. For bFROG the signal collected by the spectrometer is:

$$I_{\mathrm{bFROG}}(\tau,\omega) \propto \left| \int \left(A(t) + A(t-\tau)e^{i\phi} \right)^2 e^{2i\omega_0 t} e^{-i\omega t} dt \right|^2 \tag{27}$$

The trace features are the same as for iFROG (values at zero delay and at large delays, symmetry) but the analysis of the spectral content of the bFROG map exhibits new features. In particular, the collected signal can be expressed as a function of the centered FROG signal:

$$I_{\mathrm{bFROG}}(\tau,\omega) \propto I_{\mathrm{SH}}(\omega)\cos^2\left(\frac{\delta\omega\tau}{2}-\phi\right) + 4I^{c}_{\mathrm{FROG}}(\tau,\omega)$$

$$+8\cos\left(\frac{\delta\omega\tau}{2}-\phi\right)\mathrm{Re}\left[E^{\star}_{\mathrm{SH}}(\omega)E^{c}_{\mathrm{FROG}}(\tau,\omega)\right] \tag{28}$$

As iFROG, bFROG is the sum of three terms: a constant SH component, a FROG component -term. It also shows that if $\phi = \pi/2$ then the bFROG is almost equal to its FROG term for small delays ($\delta\omega\tau/2 \ll 1$).

4.2.1 Phase extraction

Spectral phase and amplitude cannot be retrieved from bFROG traces as from iFROG traces since the SH and FROG components are merged. However, it is still possible to retrieve this information by using a modified version of the PCGPA algorithm used for intensimetric FROG. A detailed description of this algorithm is out of the scope of this paper but, in a few words, the main modification consists in removing the SH complex amplitude prior to the projection step.

4.2.2 Experimental example

The experimental demonstration of bFROG was carried on the same visible source as described in 4.1.2. Figure 5 displays the raw experimental bFROG trace, bFROG autocorrelation and the reconstructed bFROG trace for $\phi = 0$rad. N=65 equidistant time delays covering the [-1000fs, 1000fs] interval were used for this measurement.

4.3 Phase-cycling SPIDER

4.3.1 Principle

In this variant of SPIDER, both the pulse replicas and the chirped pulse are in the same polarization state. In this case, the technique cannot be single-shot anymore. As shown below, the SPIDER signal can nevertheless be extracted by using a phase-cycling technique. For the sake of simplicity, we will consider a combination of four collinear pulses: two time-

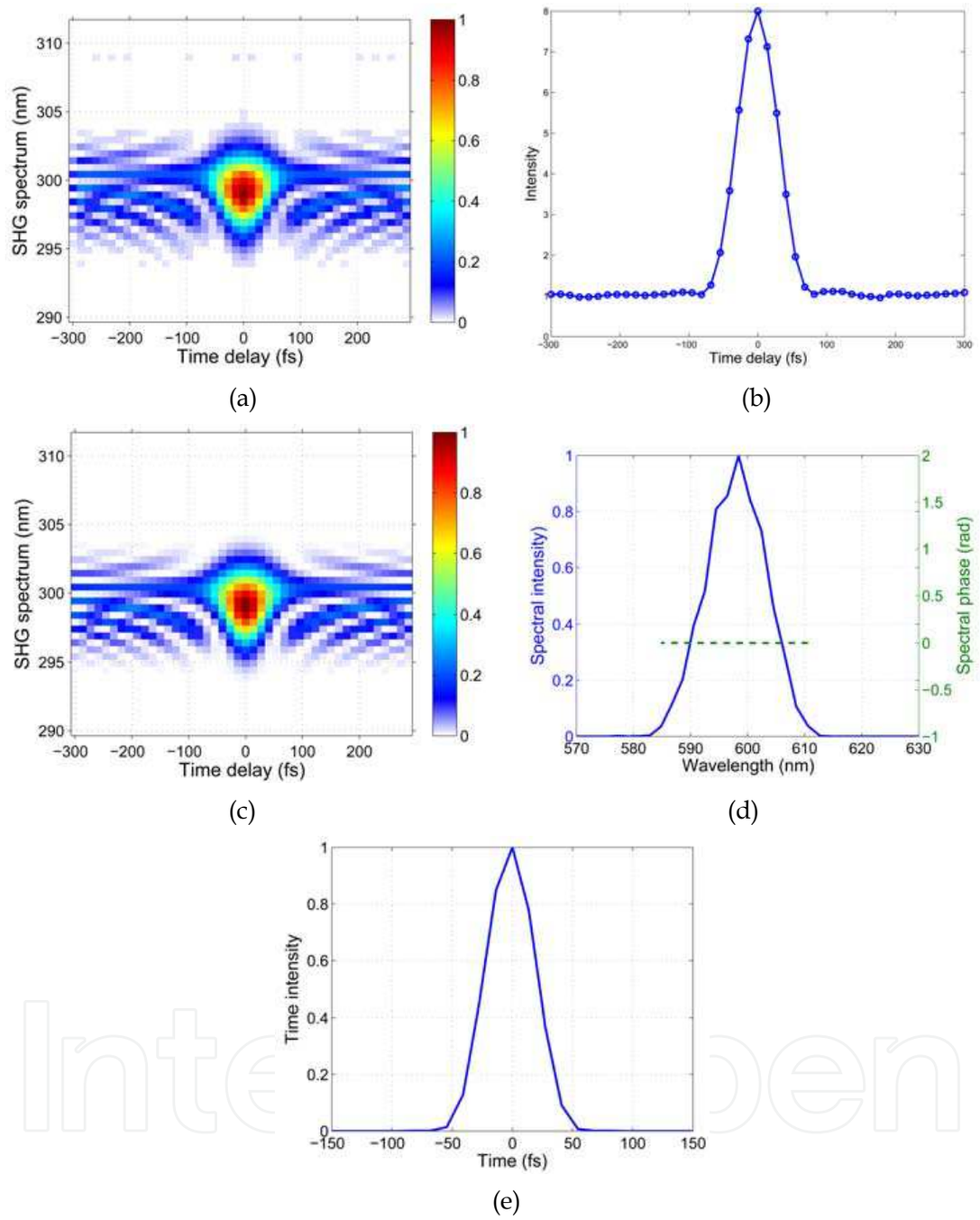

Fig. 5. a) Experimental bFROG trace. b) Experimental bFROG autocorrelation. c) Retrieved FROG trace. d) Retrieved spectral phase and intensity. e) Retrieved time intensity.

delay pulse replicas and two time-delayed quasi-monochromatic pulses (the equivalent of the two parts of the chirped pulse which overlap with the short replicas), the pulses being synchronized by pairs. The complex time-dependent amplitude of the electric fields will be noted with roman capital letters while their Fourier transforms will be noted with a hat. In the time domain, the total electric amplitude of the considered pulse combination is then:

$$E_{\text{tot}}(t) = \left\{ E(t) + M_1(t)e^{i\delta\omega t} + E(t-\tau) + M_2(t-\tau)e^{-i\delta\omega t} \right\} e^{i\omega_0 t} \tag{29}$$

The SHG signal induced by $E_{\text{tot}}(t)$ is proportional to the square of $E_{\text{tot}}(t)$. Since the pulses are much shorter than the time delay τ, cross-products of non-concomitant pulses vanish, which leads to:

$$E_{\text{tot}}^2(t) = \left\{ E^2(t) + M_1^2(t)e^{2i\delta\omega t} + M_2^2(t-\tau)e^{-2i\delta\omega t} + E_2^2(t-\tau) \right.$$

$$\left. +2E(t)M_1(t)e^{i\delta\omega t} + 2E(t-\tau)M_2(t-\tau)e^{-i\delta\omega t} \right\} e^{2i\omega_0 t} \tag{30}$$

For convenience we define:

$$E_{\text{SPIDER}}(t) = E(t)M_1(t)e^{i\delta\omega t} + E(t-\tau)M_2(t-\tau)e^{-i\delta\omega t} \tag{31}$$

This term is indeed the SPIDER signal since it corresponds to two time-delayed and spectrally shifted pulse replicas of the same pulse. The spectral amplitude of $E_{\text{tot}}^2(t)$ is then given by the Fourier transform of Equation 30:

$$\widehat{E_{\text{tot}}^2}(2\omega_0 + \Omega) = \widehat{E^2}(\Omega)\left(1 + e^{-i\Omega\tau}\right)$$

$$+\widehat{M_1^2}(\Omega - 2\delta\omega) + \widehat{M_2^2}(\Omega + 2\delta\omega)e^{-i\Omega\tau - i2\delta\omega\tau} + 2\hat{E}_{\text{SPIDER}}(\Omega) \tag{32}$$

where $\Omega = \omega - \omega_0$ is the frequency offset with respect to the central angular frequency ω_0 and $\hat{E}_{\text{SPIDER}}$ is the Fourier-transform of E_{SPIDER} which is explicitly given by:

$$\hat{E}_{\text{SPIDER}}(2\omega_0 + \Omega) = \hat{E}(\Omega) \otimes \widehat{M_1}(\Omega - \delta\omega) + \hat{E}(\Omega) \otimes \widehat{M_2}(\Omega + \delta\omega)e^{-i\Omega\tau} \tag{33}$$

Without surprise, the SHG spectral amplitude is the sum of two contributions: the individual SHGs of all fours pulses plus all the possible cross-terms. The spectral intensity, which is the only physically accessible quantity is then equal to the square modulus of Equation 32 which is a rather complicated expression. For the sake of compactness, all implicitly clear dependances with the frequency variables will be dropped from now on.

$$I_{\text{tot}}(2\omega_0 + \Omega) = \begin{cases} 4\left|\widehat{E^2}\right|^2 \cos^2(\Omega\tau) + \left|\widehat{M_1^2}\right|^2 + \left|\widehat{M_1^2}\right|^2 & \text{(SHG)} \\ +4\left|\hat{E}_{\text{SPIDER}}\right|^2 & \text{(SPIDER)} \\ +2\text{Re}\left\{\widehat{E^2}\left(1 + e^{-i\Omega\tau}\right)\left(\widehat{M_1^2} + \widehat{M_2^2}e^{-i2\Omega\tau - i2\delta\omega\tau}\right)^\star\right\} & \text{(cross-term)} \\ +4\text{Re}\left\{\hat{E}_{\text{SPIDER}}^\star\left[\widehat{E^2}\left(1 + e^{-i\Omega\tau}\right) + \widehat{M_1^2} + \widehat{M_2^2}e^{-i(\Omega+2\delta\omega)\tau}\right]\right\} & \text{(cross-term)} \end{cases} \tag{34}$$

Clearly, it is not possible to extract the SPIDER signal from $I(\omega)$, even by using a spectral filter since there are several terms oscillating with respect to $\Omega\tau$. Consequently, it is not possible to extract the SPIDER signal from this pulse combination.
We now consider the two following combinations of pulses:

$$\begin{aligned} E_{++} &= E(t) + M_1(t) + E(t-\tau) + M_2(t-\tau) \\ E_{--} &= -E(t) + M_1(t) - E(t-\tau) + M_2(t-\tau) \end{aligned} \tag{35}$$

Adding π to the phase of $E(t)$ leaves all the terms unchanged except $E_{SPIDER}(\omega)$ which becomes $-E_{SPIDER}(\omega)$. So, by summing $I_{++} = |E_{++}|^2$ and $I_{--} = |E_{--}|^2$, the SPIDER/SHG cross-term can be eliminated:

$$I_{++}+I_{--}=\begin{cases} 8\left|\widehat{E^2}\right|^2\cos^2(\Omega\tau)+2\left|\widehat{M_1^2}\right|^2+2\left|\widehat{M_1^2}\right|^2 & \text{(SHG)} \\ +8\left|\hat{E}_{SPIDER}\right|^2 & \text{(SPIDER)} \\ +4\mathrm{Re}\left\{\widehat{E^2}\left(1+e^{-i\Omega\tau}\right)\left(\widehat{M_1^2}+\widehat{M_2^2}e^{-i2\Omega\tau-i2\delta\omega\tau}\right)^{\star}\right\} & \text{(cross-term)} \end{cases} \quad (36)$$

This signal, however, still contains the parasitic term of the SHG/SHG cross term. This term is narrowband and has a minority weight but still cannot be easily removed. We now consider two additional pulse combinations:

$$\begin{aligned} E_{+-} &= E(t)+M_1(t)-E(t-\tau)+M_2(t-\tau) \\ E_{-+} &= -E(t)+M_1(t)+E(t-\tau)+M_2(t-\tau) \end{aligned} \quad (37)$$

As for I_{++} and I_{--}, summing I_{+-} and I_{-+} eliminates the cross term between the SPIDER and second harmonic terms. Next, the difference between $I_{++} + I_{--}$ and $I_{+-} + I_{-+}$ eliminates all the residual terms but one:

$$I_{++}+I_{--}-I_{+-}-I_{-+}=32\mathrm{Re}\left\{\widehat{E}(\Omega)\otimes\widehat{M_1}(\Omega-\delta\omega)\times\widehat{E}^{\star}(\Omega)\otimes\widehat{M_2}^{\star}(\Omega+\delta\omega)e^{i\Omega\tau}\right\} \quad (38)$$

Provided that the spectra of $M_1(t)$ and $M_2(t)$ are small with respect to the spectrum of $E(t)$, these spectra can be approximated by two Dirac distributions located at $+\delta\omega$ and $-\delta\omega$ and the combination of the four experimental signals can rewritten as a function of the spectral phase $\varphi(\Omega)$ of the $\hat{E}$:

$$I_{++}+I_{--}-I_{+-}-I_{-+}=32\hat{E}(\Omega+\delta\omega)\hat{E}(\Omega-\delta\omega)\cos\left(\Omega\tau+\varphi(\Omega+\delta\omega)-\varphi(\Omega-\delta\omega)\right) \quad (39)$$

This combination gives directly the term containing the spectral phase of the pulse $E(t)$.

4.3.2 Spectral filter

The spectral filter corresponding to the pulse replicas are:

$$H_1(\omega)=\exp(-i\Omega\tau/2) \quad (40)$$

$$H_2(\omega)=\exp(+i\Omega\tau/2) \quad (41)$$

and the spectral filter of the chirped pulse is given by:

$$H_3(\omega)=\mathrm{Rect}\left(\omega_0,\Delta\omega\right)\exp(i\phi^{(2)}\Omega^2/2) \quad (42)$$

The spectral filter is then given by the sum of three filters:

$$H_{\pm\pm}(\omega)=\pm H_1(\omega)\pm H_2(\omega)+H_3(\omega) \quad (43)$$

In these formula, $\Omega = \omega - \omega_0$ stands for the frequency offset from the carrier frequency, $\phi^{(2)}$ is the second order phase (chirp) coefficient and Rect (ω_0,$\Delta\omega$) is a passband amplitude function

of width $\Delta\omega$ located at frequency ω_0. The mean group delays of the chirped pulse and of the double pulse structure are equal, which is one of the two conditions required to have a non zero time overlap between the chirped pulse and the pulse replicas. The other condition is to choose large enough values for the chirp coefficient $\phi^{(2)}$ and the bandwidth $\Delta\omega$ so that the temporal spread of the chirped pulse is greater than the interpulse delay. In practice however, there is almost no degree of freedom since the optimal ratio $\tau/\phi^{(2)} = \delta\omega$, which corresponds to the spectral shear between the pulse replicas after the SH stage, must be chosen as small as possible but cannot be smaller than the spectral resolution of the AOPDF.

4.3.3 Experimental demonstration

The experimental demonstration of cSPIDER was also carried on the same visible source as described in subsubsection 4.1.2. The interpulse delay was set to 500fs and the spectral shear to 2nm at 600nm. Figure 6 shows the raw acquired spectra together with the extracted signals.
The SPIDER signal, extracted using formula 39, is shown in Figure 6c.

4.4 Homodyme phase-cycling SPIDER

4.4.1 Principle

Homodyne SPIDER (hSPIDER) is a version of SPIDER that uses a self-referencing homodyne detection. This technique has a higher sensitivity than phase-cycling SPIDER and is self-calibrated with regard to the exact value of the interpulse delay τ.
In the world of pulse measurements, the most sensitive method demonstrated to date is spectral interferometry, in which a high-energy well-characterized reference pulse interferes with a weak unknown pulse in a spectrometer. The primary advantage of this technique over self-referencing approaches is the use of homodyne detection: a strong local oscillator provides effective amplification of the weak signal field due to the properties of square-law detectors. On the other hand, the main drawback is the need for detailed knowledge of the local oscillator pulse field (reference pulse), which increases the complexity of the method since an ancillary measurement of the reference pulse is necessary.
The homodyne implementation of SPIDER takes advantage of homodyne detection, while retaining the self-referencing and direct inversion features that are the hallmarks of its simplicity. The method is based on the interference of frequency-sheared replicas of the input pulse with an uncharacterized high-energy reference pulse, which is the SH signal of the pulse to be measured. In hSPIDER, one of the upshifted pulse replicas is replaced by the SH of the input pulse. Let ω_1 be the frequency shift of the upshifted pulse replica with respect to the input pulse and $\varphi_{SHG}(\omega)$ the spectral phase of the SH of the input pulse. The FTSI of the resulting signal is then:

$$\phi_{hSPIDER,1}(\omega) = \omega\tau + \varphi(\omega + \omega_1) - \varphi_{SHG}(\omega) \tag{44}$$

The spectral phase of the input pulse cannot be directly retrieved since the spectral phase of the SH is unknown. However, with two different frequency shifts, both the linear term $\omega\tau$ and the SHG phase term can be eliminated. hSPIDER measurement hence requires three steps: measurement of the phase difference between the SH and a pulse replica upshifted by ω_1, measurement of the phase difference between the SH and a pulse replica upshifted by ω_2, computation of the difference between these two homodyne phases.

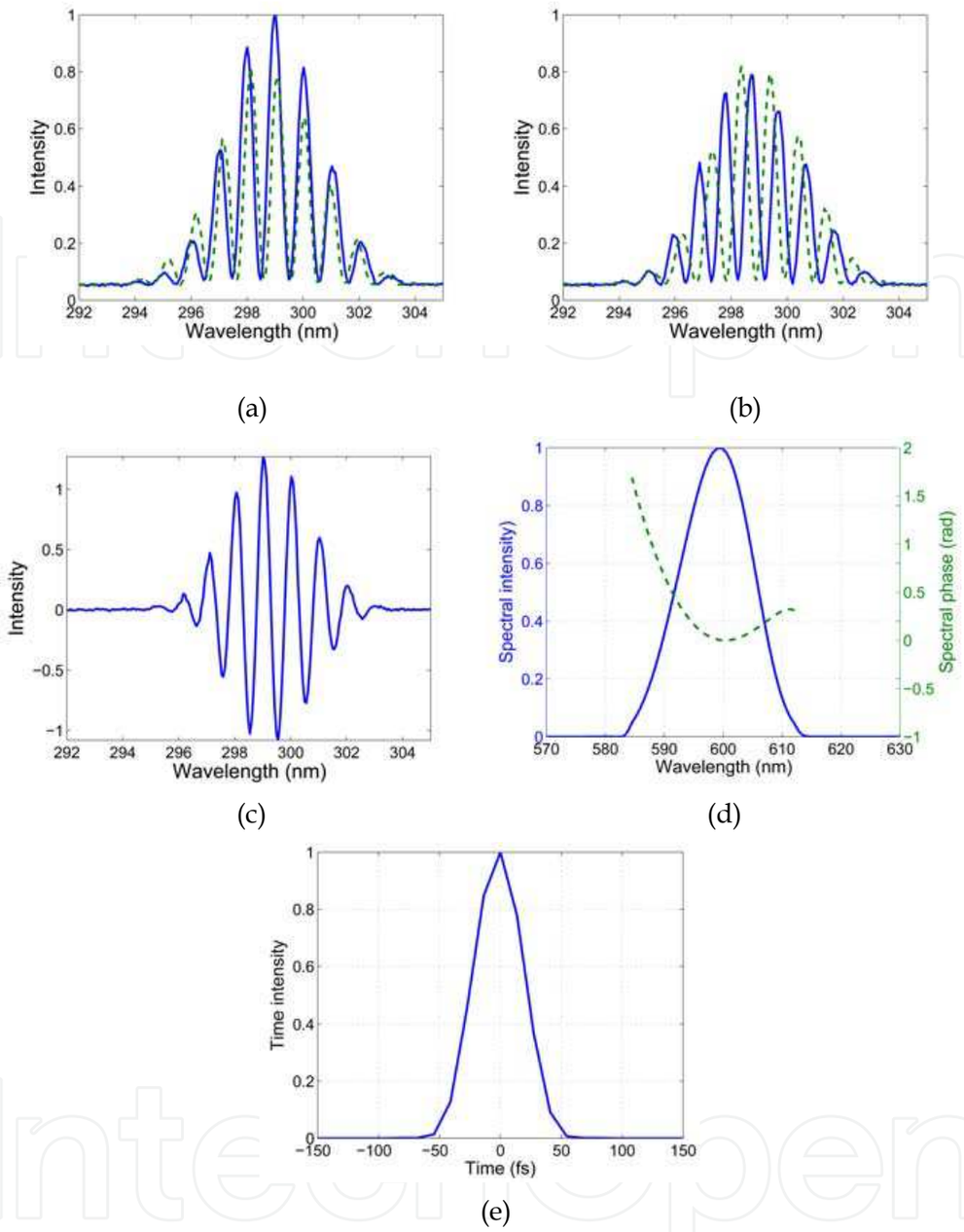

Fig. 6. cSPIDER experimental results. a) $I_{++}(\omega)$ (solid line) and $I_{--}(\omega)$ (dashed line). b) $I_{+-}(\omega)$ (solid line) and $I_{-+}(\omega)$ (dashed line). c) Extracted SPIDER signal. d) Retrieved spectrum and spectral phase. e) Retrieved time intensity.

The resulting phase function is then:

$$\Delta\phi(\omega) = \phi_{\text{hSPIDER},2}(\omega) - \phi_{\text{hSPIDER},1}(\omega) = \varphi(\omega + \omega_2) - \varphi(\omega + \omega_1) \tag{45}$$

which, by concatenation and global shift, yields eventually the spectral phase $\varphi(\omega)$.
As for cSPIDER, it is not possible to generate an isolated upshifted pulse replica by using a single beam and a single polarization state. However, it is possible to extract the relevant

signal by phase-cycling. For hSPIDER, the relevant combination of pulses is the following: two time-delayed pulse replicas and *one* time-delayed quasi-monochromatic pulse. This narrowband pulse is synchronized with one of the pulse replicas and doesn't overlap with the other pulse replica. The total electric field then reads:

$$E_{\pm 1}(t) = \left\{ E(t) + E(t-\tau) \pm M_1(t-\tau) e^{-i\delta\omega_1 t} \right\} e^{i\omega_0 t} \tag{46}$$

In the time domain, the SHG signal induced by $E_{\pm,1}(t)$ is proportional to the square of $E_{\pm,1}(t)$. Since the pulses are much shorter than the interpulse delay τ, the cross-product between the first pulse replica and the narrowband pulse vanishes, which leads to the following expression:

$$E_{\pm 1}^2(t) = \left\{ E^2(t) + M_1^2(t-\tau) e^{-2i\delta\omega_1 t} + E^2(t-\tau) \pm 2E(t-\tau) M_1(t-\tau) e^{-i\delta\omega_1 t} \right\} e^{i2\omega_0 t} \tag{47}$$

The SH spectral intensity is then equal to the square modulus of Equation 47 which can be written as follows:

$$I_{\pm 1}(2\omega_0 + \Omega) = \begin{cases} \left| \widehat{E^2}(\Omega) \pm 2\widehat{E}(\Omega) \otimes \widehat{M_1}(\Omega - \delta\omega_1) e^{-i\Omega\tau} \right|^2 \\ + \left| \widehat{M_1^2}(\Omega - 2\delta\omega_1) e^{-i\Omega\tau} + \widehat{E^2}(\Omega) e^{-i\Omega\tau} \right|^2 \\ + 2\mathrm{Re} \left\{ \left(\widehat{E^2}(\Omega) \pm 2\widehat{E}(\Omega) \otimes \widehat{M_1}(\Omega - 2\delta\omega_1) e^{-i\Omega\tau} \right) \right. \\ \left. \times \left(\widehat{M_1^2}(\Omega - \delta\omega_1) + \widehat{E^2}(\Omega) \right)^{\star} e^{i\Omega\tau} \right\} \end{cases} \tag{48}$$

In Equation 48, the first term is the homodyne SPIDER term, the second term is the SHG parasitic background, and the third term is the cross-product of these two contributions. By summing I_{+1} and I_{-1}, the SHG parasitic background can be eliminated:

$$\begin{aligned} I_{+1} - I_{-1} = {} & 8\mathrm{Re} \left\{ \widehat{E^2}^{\star}(\Omega) \times \left[\widehat{E}(\Omega) \otimes \widehat{M_1}(\Omega - \delta\omega_1) e^{-i\Omega\tau} \right] \right\} \\ & + 8\mathrm{Re} \left\{ \widehat{E}(\Omega) \otimes \widehat{M_1}(\Omega - \delta\omega_1) \left(\widehat{M_1^2}(\Omega - 2\delta\omega_1) + \widehat{E^2}(\Omega) \right)^{\star} \right\} \end{aligned} \tag{49}$$

The combination still contains two terms however: the homodyne SPIDER term, which is an oscillating term with respect to Ω, and a DC term. A Fourier filter around the beat "frequency" τ is, therefore, able to isolate the homodyne term. By using FTSI, it is possible to retrieve, assuming that the narrowband pulse is of negligible width:

$$\phi_{\mathrm{hSPIDER},1}(\omega) = -\Omega\tau + \varphi(\omega + \omega_1) - \varphi_{\mathrm{SHG}}(\omega) \tag{50}$$

By repeating this measurement with another frequency shear, that is with the pulse combinations

$$E_{\pm,2}(t) = \left\{ E(t) + E(t-\tau) \pm M_2(t-\tau) e^{-i\delta\omega_2 t} \right\} e^{i\omega_0 t} \tag{51}$$

another homodyne signal can be extracted:

$$\phi_{\mathrm{hSPIDER},2}(\omega) = -\Omega\tau + \varphi(\omega + \omega_2) - \varphi_{\mathrm{SHG}}(\omega) \tag{52}$$

By combining $\phi_{hSPIDER,1}$ and $\phi_{hSPIDER,2}$, the derivative of the spectral phase $\varphi(\omega)$ can be retrieved.

4.4.2 Experimental demonstration

The experimental demonstration of hSPIDER was also carried on the same visible source as described in subsubsection 4.1.2. The interpulse delay was set to 600fs and the spectral shear to 2nm at 600nm. Figure 7 shows the raw acquired spectra together with the extracted signals.

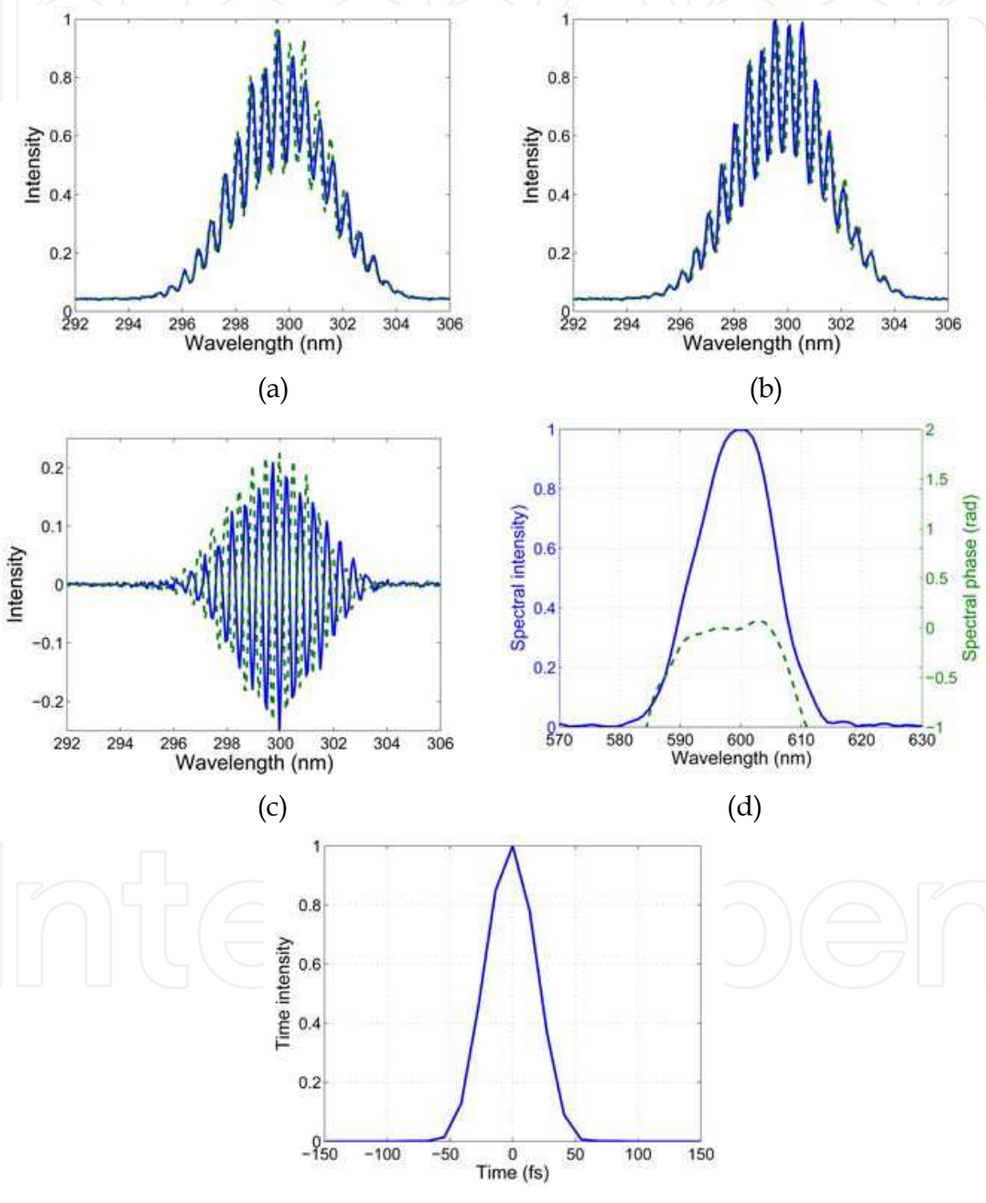

Fig. 7. hSPIDER experimental results. a) $I_{+1}(\omega)$ (solid line) and $I_{-1}(\omega)$ (dashed line). b) $I_{+2}(\omega)$ (solid line) and $I_{-2}(\omega)$ (dashed line). c) Extracted homodyne signals. d) Retrieved spectral phase and intensity. e) Retrieved time intensity.

5. Cross-check

As it was stressed in the introduction, pulse shapers offer the unique possibility to crosscheck between several pulse measurements. All the experiments reported in section 4 have been performed with the same OPA source and can be therefore be compared. The retrieved time intensity from iFROG, bFROG, cSPIDER and hSPIDER measurements are compared in Figure 8. As can be seen, all four pulse measurements agree on the pulse duration as well as on the time shape. On the other hand, Figure 9 is an example of non-consistent measurements. The experiment was performed at ~800nm on a kHz amplified system delivering pulses of ~25fs. A fraction of the output beam was sampled and sent to a thin Calcite plate and then to a Glan polarizer. The Calcite crystal was orientated so that the angle between the input polarization and the principal polarization plane was close to 45 degrees. The group delay between the ordinary and extraordinary polarizations was independently measured to be ~80fs. The polarizer was set to transmit the initial polarization, so that, after propagation through the Calcite plate and the polarizer, a double pulse structure was generated. This double pulse was characterized by both FROG and SPIDER measurements and the result of these measurements is displayed in Figure 9. As can be noted, both measurements retrieve this double structure with the correct interpulse delay but the SPIDER measurement shows a spurious post pulse, whereas the FROG measurement doesn't. This was the result of a bad choice of parameters for the SPIDER measurement: the chosen interpulse delay (300fs) was too small to characterize a 100fs pulse structure.

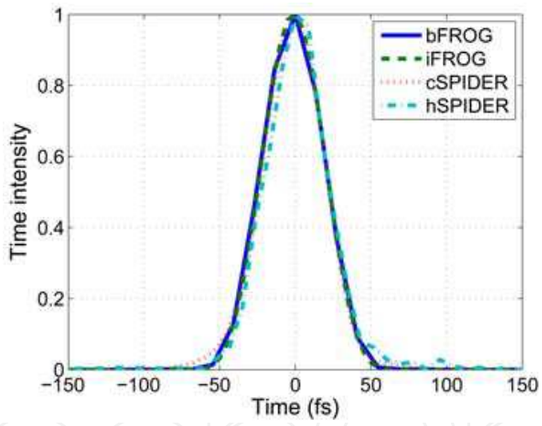

Fig. 8. Compared time intensities retrieved by bFROG, iFROG, cSPIDER and hSPIDER.

6. Extension to the UV

Ultrashort pulse characterization techniques based on second harmonic generation (SHG), such as frequency resolved optical gating (SH-FROG), were developed for the near infrared and cannot be easily transposed to the UV and the visible range because of the lack of suitable and efficient non linear crystals for broadband SHG. Such difficulties can be overcome by the use of a third order non linear effect such as induced birefringence which is achromatic and frequency conserving. However, third order non linear effects usually require non collinear geometry in order to allow the extraction of the useful signal, which greatly increases the complexity of the system. Conversely, a single-beam geometry would greatly simplify the optical setup but comes at the expense of an interferometric control of the delay between pulse replicas and signal discrimination.

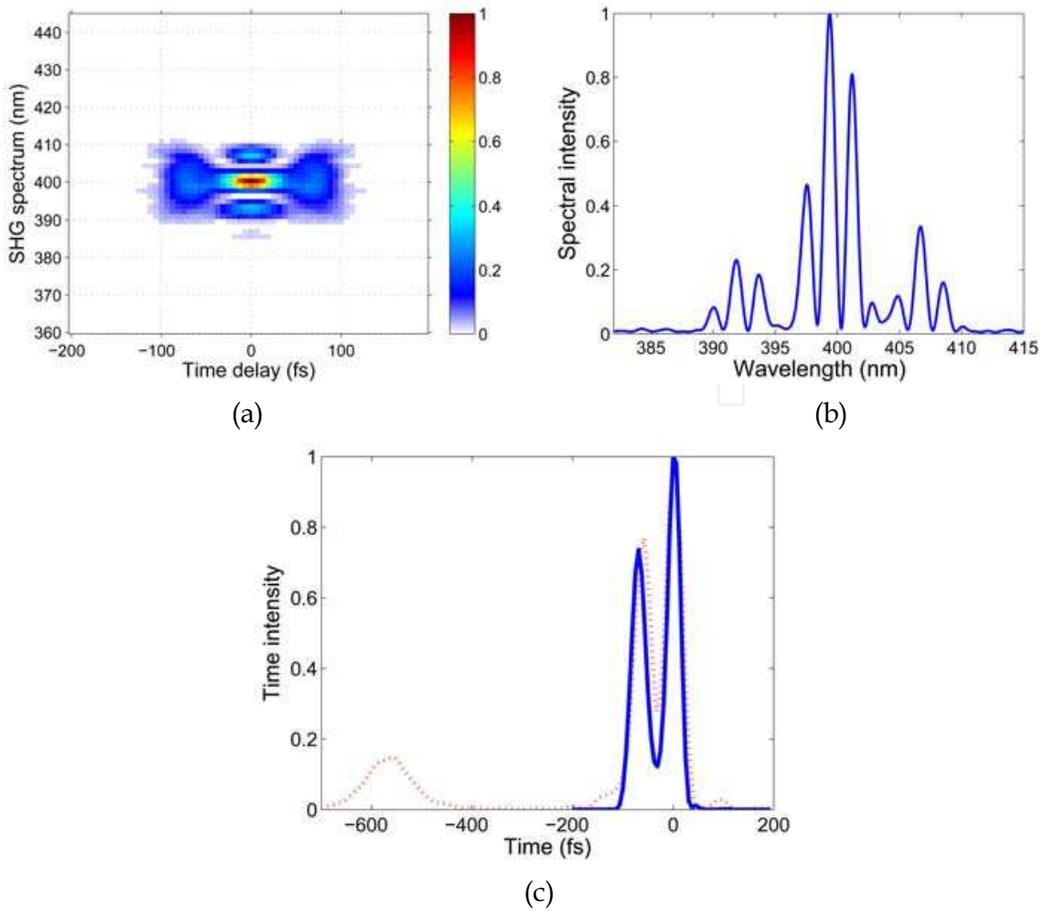

(a) (b)

(c)

Fig. 9. a) Experimental FROG traces. b) Experimental SPIDER spectrum. c) Compared retrieved time intensities (FROG: solid line. SPIDER: dots).

In this section we demonstrate a single beam, achromatic, programmable and self-compensated spectrally resolved interferometric autocorrelation technique which overcomes such drawbacks. This technique is based on the conjugate use of UV acousto-optic programmable dispersive filter (UV-AOPDF, Coudreau et al. (2006)) and of a recently discovered third order non linear effect, cross-polarized wave (XPW) generation (Canova et al., 2008; Jullien et al., 2005).

6.1 Cross-polarized wave generation

Under a strong illumination by a linearly polarized wave, a nonlinear crystal with an anisotropic cubic susceptibility can generate a cross-polarized wave at the same wavelength as the incident wave. The intensity of the generated XPW signal varies as the cubic power of the intensity of the input wave. Barium fluoride (BaF2) is especially well adapted to XPW generation. First, its high $\chi^{(3)}$ anisotropy allows for good conversion efficiency. Second, its linear optical properties allow for perfect group-velocity matching along the propagating axis and, as a consequence, for a perfect spatial overlap of the cross-polarized waves. Assuming that two replicas of an ultrashort optical pulse $E(t)$ with an interpulse delay τ are incident on the non linear crystal, the XPW intensity writes:

$$I_{\mathrm{XPW}}(\tau) \propto \int \left(E(t) + E(t-\tau)\right)^3 dt \tag{53}$$

When spectrally resolved, this signal contains, in theory, all the information required to retrieve the spectral phase and amplitude of $E(t)$.

6.2 Setup and proof of principle

The UV-AOPDF (75mm-long KDP crystal) is set to produce a pair of replicas of the input short pulse $E(t)$ and to vary the interpulse delay while maintaining a constant carrier envelope phase. The diffracted beams are focused into a 3mm thick BaF_2 crystal by a first lens and recollimated by a second lens. A Glan polarizer is used to isolate the XPW signal and a spectrometer records the XPW spectrum (Figure 10). The AOPDF is also used to precompensate the optical dispersion of all optical elements: lenses, KDP and BaF_2 crystals.

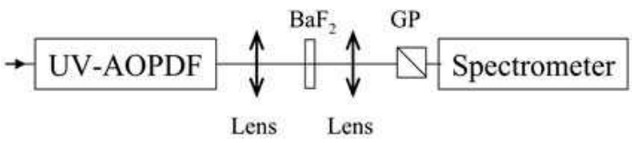

Fig. 10. Experimental setup (GP: Glan polarizer).

First experiments were performed on the SHG output of an amplified Ti:Sapphire system delivering Fourier-transform limited pulses of 40fs at 397nm. The bFROG trace is shown in Figure 11a along with the derived autocorrelation function and shows a good agreement with the expected pulse width. The experimental bFROG trace of a double pulse structure

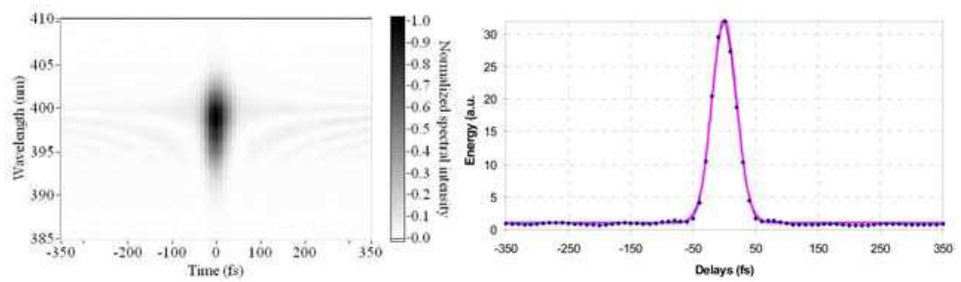

(a) Single pulse.

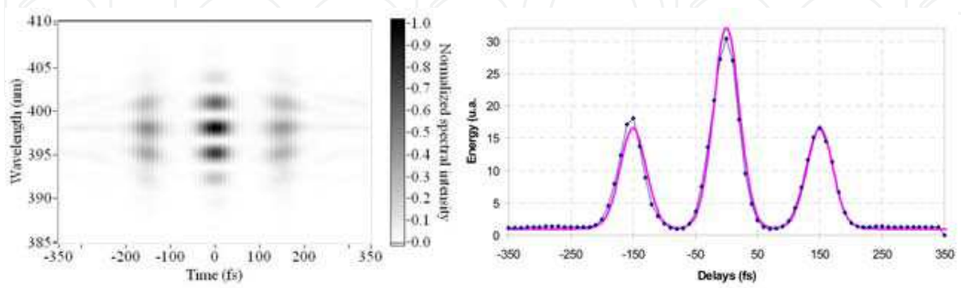

(b) Doublepulse

Fig. 11. a) Experimental bFROG trace (left) and autocorrelation (right) of the 40fs UV pulses. b) Experimental bFROG trace (left) and autocorrelation (right) of a double UV pulse with interpulse delay of 150fs. Dots: experimental. Solid line: theory.

with a pulse separation of 150fs is shown in Figure 11b. The bFROG trace exhibits the double pulse structure as well as the expected spectral modulations with excellent agreement with the theoretical interpulse delay. The XPW conversion efficiency was not measured exactly, but was estimated to be of the order of 1%. Given the extinction ratio of the polarizer (10^4), the signal to background ratio is estimated to better than 100.

7. Conclusion

In this chapter we explored the practical implementation of several pulse characterization techniques on a minimal optical setup comprising an AOPDF, an SHG stage and a spectrometer. Although special interest was brought to SPIDER and SH-FROG related techniques, we demonstrated that two-filter techniques can be made single-filter by slight adaptations. We introduced new pulse measurement techniques (bFROG, cSPIDER, hSPIDER), provided experimental demonstrations of these methods and performed a mutual cross-check. Finally, we showed how some of these techniques could be extended to the near UV spectral range by using a third order nonlinear effect.

8. References

Albrecht, A. W., Hybl, J. D., Faeder, S. M. G. & Jonas, D. M. (1999). Experimental distinction between phase shifts and time delays: Implications for femtosecond spectroscopy and coherent control of chemical reactions, *Journal Of Chemical Physics* 111(24): 10934– 10956.

Amat-Roldan, I., Cormack, I. G., Loza-Alvarez, P. & Artigas, D. (2005). Measurement of electric field by interferometric spectral trace observation, *Optics Letters* 30(9): 1063–1065.

Amat-Roldan, I., Cormack, I., Loza-Alvarez, P., Gualda, E. & Artigas, D. (2004). Ultrashort pulse characterisation with shg collinear-frog, *Opt. Express* 12(6): 1169–1178.
URL: *http://www.opticsexpress.org/abstract.cfm?URI=oe-12-6-1169*

Canova, L., Kourtev, S., Minkovski, N., Lopez-Martens, R., Albert, O. & Saltiel, S. M. (2008). Cross-polarized wave generation in the uv region, *Opt. Lett.* 33(20): 2299–2301.
URL: *http://ol.osa.org/abstract.cfm?URI=ol-33-20-2299*

Coudreau, S., Kaplan, D. & Tournois, P. (2006). Ultraviolet acousto-optic programmable dispersive filter laser pulse shaping in kdp, *Opt. Lett.* 31(12): 1899–1901.
URL: *http://ol.osa.org/abstract.cfm?URI=ol-31-12-1899*

DeLong, K. W., Fittinghoff, D. N., Trebino, R., Kohler, B. & Wilson, K. (1994). Pulse retrieval in frequency-resolved optical gating based on the method of generalized projections, *Opt. Lett.* 19(24): 2152–2154.
URL: *http://ol.osa.org/abstract.cfm?URI=ol-19-24-2152*

Fittinghoff, D., Squier, J., Barty, C., Sweetser, J., Trebino, R. & Muller, M. (1998). Collinear type ii second-harmonic-generation frequency-resolved optical gating for use with high-numerical-aperture objectives, *Optics letters* 23(13): 1046–1048.

Forget, N., Coudreau, S., Lepetit, F., Albert, O. & Oksenhendler, T. (2007). Achromatic and single-beam pulse characterization technique for visible-uv pulses based on direct uv pulse shaping and cross-polarized wave generation, *CLEO/Europe and IQEC 2007 Conference Digest*, Optical Society of America, pp. CF4–5.

Forget, N., Joffre, M., Coudreau, S. & Oksenhendler, T. (2007). Toward programmable ultrashort pulse characterization, *CLEO/Europe and IQEC 2007 Conference Digest*, Optical Society of America, pp. CF–16.

Froehly, C., Colombeau, B. & Vampouille, M. (1983). Shaping and analysis of picosecond light pulses, *Progress in optics* 20: 63–153.

Galler, A. & Feurer, T. (2008). Pulse shaper assisted short laser pulse characterization, *Applied Physics B: Lasers and Optics* 90(3): 427–430.

Gallmann, L., Steinmeyer, G., Sutter, D. H., Matuschek, N. & Keller, U. (2000). Collinear type ii second-harmonic-generation frequency-resolved optical gating for the characterization of sub-10-fs optical pulses, *Opt. Lett.* 25(4): 269–271.
URL: *http://ol.osa.org/abstract.cfm?URI=ol-25-4-269*

Garzella, D., Lepetit, F., Gobert, O., Perdrix, M., Hollander, P. & Oksenhendler, T. (2006). Temporal analysis ans shape control of uv high energy laser pulses for photoinjector, *Proc. FEL 2006*, number THPPH001, pp. 552–555.

Grabielle, S., Forget, N., Coudreau, S., Oksenhendler, T., Kaplan, D., Hergott, J.-F. & Gobert, O. (2009). Local spectral compression method for cpa lasers, *CLEO/Europe and EQEC 2009Conference Digest*.

Iaconis, C. & Walmsley, I. (1998). Spectral phase interferometry for direct electric-field reconstruction of ultrashort optical pulses, *Opt. Lett.* 23(10): 792–794.
URL: *http://ol.osa.org/abstract.cfm?URI=ol-23-10-792*

Jullien, A., Albert, O., Ch´eriaux, G., Etchepare, J., Kourtev, S., Minkovski, N. & Saltiel, S. M. (2005). Nonlinear polarization rotation of elliptical light in cubic crystals, with application to cross-polarized wave generation, *J. Opt. Soc. Am. B* 22(12): 2635–2641.
URL: *http://josab.osa.org/abstract.cfm?URI=josab-22-12-2635*

Kane, D., Inc, S. & Santa Fe, N. (1999). Recent progress toward real-time measurement of ultrashort laserpulses, *IEEE Journal of Quantum Electronics* 35(4): 421–431.

Lozovoy, V., Pastirk, I. & Dantus, M. (2004). Multiphoton intrapulse interference. iv. Ultrashort laser pulse spectral phase characterization and compensation, *Optics letters* 29(7): 775–777.

Monmayrant, A., Joffre, M., Oksenhendler, T., Herzog, R., Kaplan, D. & Tournois, P. (2003). Time-domain interferometry for direct electric-field reconstruction by use of an acousto-optic programmable filter and a two-photon detector, *Opt. Lett.* 28(4): 278–280.
URL: *http://ol.osa.org/abstract.cfm?URI=ol-28-4-278*

Murphy, D. S., McKenna, J., Calvert, C. R., Bryan, W. A., English, E. M. L., Wood, J., Turcu, I. C. E., Newell, W. R., Williams, I. D. & McCann, J. F. (2007). Controlling dissociation processes in the d-2(+) molecular ion using high-intensity, ultrashort laser pulses, *JOURNAL OF PHYSICS B-ATOMIC MOLECULAR AND OPTICAL PHYSICS* 40(11): S359–S372.

Ogilvie, J. P., Débarre, D., Solinas, X., Martin, J.-L., Beaurepaire, E. & Joffre, M. (2006). Use of coherent control for selective two-photon fluorescence microscopy in live organisms, *Opt. Express* 14(2): 759–766.
URL: *http://www.opticsexpress.org/abstract.cfm?URI=oe-14-2-759*

Ohno, K., Tanabe, T. & Kannari, F. (2002). Adaptive pulse shaping of phase and amplitude of an amplified femtosecond pulse laser by direct reference to frequency-resolved optical gating traces, *JOSAB* 19(11): 2781–2790.

Oksenhendler, T., Monmayrant, A., Herzog, R., Kaplan, D., Tournois, P. & Joffre, M. (2003). Time-domain interferometry for direct electric-field reconstruction by use of an acousto-optic programmable dispersive filter, *in* D. Miller, M. Murnane, N. Scherer & A. Weiner (eds), *ULTRAFAST PHENOMENA XIII*, Vol. 71 of *SPRINGER SERIES IN CHEMICAL PHYSICS*, pp. 220–222. 13th International Conference on Ultrafast Phenomena, VANCOUVER, CANADA, MAY 12-17, 2002.

Reid, D. (1999). Algorithm for complete and rapid retrieval of ultrashort pulseamplitude and phase from a sonogram, *IEEE Journal of Quantum Electronics* 35(11): 1584–1589.

Seres, E., Herzog, R., Seres, J., Kaplan, D. & Spielmann, C. (2003). Generation of intense 8 fs laser pulses, *Opt. Express* 11(3): 240–247.

Stibenz, G., Ropers, C., Lienau, C., Warmuth, C., Wyatt, A. S., Walmsley, I. A. & Steinmeyer, G. (2006). Advanced methods for the characterization of few-cycle light pulses: a comparison, *Applied Physics B-Lasers And Optics* 83(4): 511–519.

Stibenz, G. & Steinmeyer, G. (2005). Interferometric frequency-resolved optical gating, *Optics Express* 13(7): 2617–2626.

Sung, J., Chen, B.-C. & Lim, S.-H. (2008). Single-beam homodyne spider for multiphoton microscopy, *Opt. Lett.* 33(13): 1404–1406.
URL: *http://ol.osa.org/abstract.cfm?URI=ol-33-13-1404*

Tkaczyk, E. R., Mauring, K., Tkaczyk, A. H., Krasnenko, V., Ye, J. Y., Jr., J. R. B. & Norris, T. B. (2008). Control of the blue fluorescent protein with advanced evolutionary pulse shaping, *Biochemical and Biophysical Research Communications* 376(4): 733 – 737.
URL: *http://www.sciencedirect.com/science/article/B6WBK-4THJ4HB-2/2/478cac9116090743c2a2ea82be5b4970*

Tournois, P. (1997). Acousto-optic programmable dispersive filter for adaptive compensation of group delay time dispersion in laser systems, *Opt. Commun.* 140(4-6): 245–249.

Trebino, R., DeLong, K. W., Fittinghoff, D. N., Sweetser, J. N., Krumbugel, M. A., Richman, B. A. & Kane, D. J. (1997). Measuring ultrashort laser pulses in the timefrequency domain using frequency-resolved optical gating, *Review Of Scientific Instruments* 68(9): 3277–3295.

Verluise, F., Laude, V., Cheng, Z., Spielmann, C. & Tournois, P. (2000). Amplitude and phase control of ultrashort pulses by use of an acousto-optic programmable dispersive filter: pulse compression and shaping, *Opt. Lett.* 25(8): 575–577.

Veshapidze, G., Trachy, M., Jang, H., Fehrenbach, C. & DePaola, B. (2007). Pathway for twocolor photoassociative ionization with ultrafast optical pulses in a rb magneto-optical trap, *Physical Review A* 76(5): 51401.

von Vacano, B., Buckup, T. & Motzkus, M. (2006). In situ broadband pulse compression for multiphoton microscopy using a shaper-assisted collinear spider, *Optics Letters* 31(8): 1154–1156.

von Vacano, B., Buckup, T. & Motzkus, M. (2007). Shaper-assisted collinear spider: fast and simple broadband pulse compression in nonlinear microscopy, *J. Opt. Soc. Am. B* 24(5): 1091–1100.
URL: *http://josab.osa.org/abstract.cfm?URI=josab-24-5-1091*

Walmsley, I. & Dorrer, C. (2009). Characterization of ultrashort electromagnetic pulses, *Advances in Optics and Photonics* 1(2): 308–437.

Weiner, A. (2000). Femtosecond pulse shaping using spatial light modulators, *Review of Scientific Instruments* 71: 1929.

Wong, V. &Walmsley, I. A. (1995). Linear filter analysis of methods for ultrashort-pulse-shape measurements, *Journal Of The Optical Society Of America B-Optical Physics* 12(8): 1491– 1499.

Yamada, H., Yokoyama, K., Teranishi, Y., Sugita, A., Shirai, T., Aoyama, M., Akahane, Y., Inoue, N., Ueda, H., Yamakawa, K., Yokoyama, A., Kawasaki, M. & Nakamura, H. (2005). Selective transition to the closely-lying states cs(7d(3/2)) and cs(7d(5/2)) by femtosecond laser pulses, *Phys.Rev.A* 72(6): 000.

Advances in Solid State Lasers Development and Applications

Edited by Mikhail Grishin

ISBN 978-953-7619-80-0
Hard cover, 630 pages
Publisher InTech
Published online 01, February, 2010
Published in print edition February, 2010

Invention of the solid-state laser has initiated the beginning of the laser era. Performance of solid-state lasers improved amazingly during five decades. Nowadays, solid-state lasers remain one of the most rapidly developing branches of laser science and become an increasingly important tool for modern technology. This book represents a selection of chapters exhibiting various investigation directions in the field of solid-state lasers and the cutting edge of related applications. The materials are contributed by leading researchers and each chapter represents a comprehensive study reflecting advances in modern laser physics. Considered topics are intended to meet the needs of both specialists in laser system design and those who use laser techniques in fundamental science and applied research. This book is the result of efforts of experts from different countries. I would like to acknowledge the authors for their contribution to the book. I also wish to acknowledge Vedran Kordic for indispensable technical assistance in the book preparation and publishing.

INTECH
open science | open minds

InTech Europe
University Campus STeP Ri
Slavka Krautzeka 83/A
51000 Rijeka, Croatia
Phone: +385 (51) 770 447
Fax: +385 (51) 686 166
www.intechopen.com

InTech China
Unit 405, Office Block, Hotel Equatorial Shanghai
No.65, Yan An Road (West), Shanghai, 200040, China
中国上海市延安西路65号上海国际贵都大饭店办公楼405单元
Phone: +86-21-62489820
Fax: +86-21-62489821

IntechOpen